Langmuir

ARTICLE

pubs.acs.org/Langmuir

Influence of Cationic Composition and pH on the Formation of Metal Stearates at Oil−Water Interfaces

Riëlle de Ruiter,* R. Willem Tjerkstra, Michèl H. G. Duits, and Frieder Mugele

Physics of Complex Fluids, Faculty of Science and Technology, IMPACT and MESA+ Institutes, University of Twente, P.O. Box 217, 7500 AE Enschede, The Netherlands

Supporting Information

ABSTRACT: We study the formation of layers of metal stearates at the interface between a decane solution of stearic acid and aqueous salt solutions of variable composition and pH by monitoring the evolution of their mechanical, optical, and chemical properties as a function of time after formation of the interface. For values of the pH below the pK_a of stearic acid hardly any interfacial activity is observed. For pH > pK_a, stearic acid deprotonates at the interface and forms metal stearates, eventually leading to the formation of macroscopic solid layers. Dynamic interfacial tension measurements reveal that the process takes place in several stages, which we attribute to the successive formation of dilute and dense monolayers followed by three-dimensional growth. In the presence of divalent ions, the solid layers display a significant increase in the dilatational storage modulus. Experiments performed with an aqueous phase containing multiple cation species (artificial seawater) give rise to particularly pronounced growth of solid layers, which preferentially incorporate Ca^{2+} as revealed by X-ray photoelectron and infrared spectroscopy. Our results highlight in particular the importance of the complex synergistic effects of simultaneously present monovalent and divalent cation species on the interfacial adsorption.

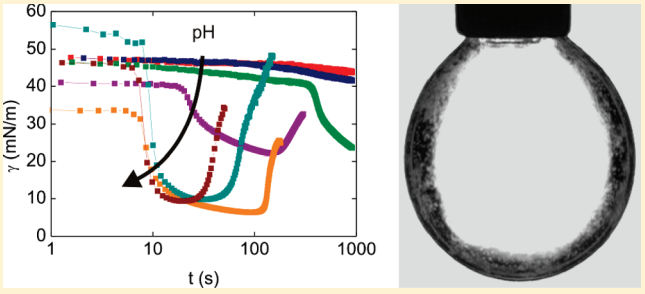

1. INTRODUCTION

The formation of adsorbed layers at oil/water interfaces can have a strong influence on the stability of emulsions as well as on the flow of two-phase fluids in microchannels or porous media. This makes it an interesting case from both fundamental scientific and application oriented viewpoints. Application areas include geology and environmental sciences, biology, and food science.

A prominent example is found in oil recovery, where such layer formation can cause problems. Here, the extensive contact between crude oil and injection water allows organic acids from the oil to react across the interface with cations in the water. This leads to the formation of interfacial layers of metal soaps, which can then act as stabilizers for emulsified oil drops. Such an emulsification can seriously hamper the oil−water separation. In addition, also solid agglomerates of metal stearates can be formed, leading to blockage of pores in the rock.[1,2] Besides problems, interfacial layer formation can also offer opportunities. Examples hereof are found in the food industry, where microscopic bubbles or droplets are stabilized using solidlike layers of proteins, polymers, or particles. In connection to these applications, also fundamental studies have been performed, focusing at either planar[3,4] or curved[5−8] interfaces.

However, relatively few studies have been aimed at the *in situ* formation of interfacial solid layers via reaction, nucleation, and growth processes at the oil/water interface.[9−11] More insight into the formation mechanism and the physical properties of such layers is therefore needed: both to solve problems with unwanted layer formation and to enable possible new applications, like droplets or bubbles coated with a layer of tunable thickness and/or mechanical properties.

An obstacle in obtaining such insights, especially in biologically and geologically oriented studies, is the enormous complexity generated by the composition of the involved materials. These compositions are often dictated by practice. For example, most biological cells (stabilized by lipid bilayers) need to be in an environment that contains various ions in a specific composition. Even slight disturbances thereof can cause the cell to disfunction or die. Another example is found in oil recovery, where crude oil containing a variety of complex molecules with diverse physicochemical properties[12−14] is exposed to aqueous fluid containing many different ions. In this case the ionic composition of the water can be adapted to increase the recovery efficiency.[15,16] However, the mechanism(s) underlying this effect are still poorly understood.

These examples underline the need to address the role of phase composition in the formation of interfacial layers. Again, relatively few studies have been performed. Most of the existing work is focused on comparing different individual ions in their effects on surfactant adsorption and/or layer formation. Examples are the papers by Brandal et al.[1,17] and Havre et al.,[2] who studied the

Received: March 21, 2011
Revised: May 31, 2011
Published: June 16, 2011

formation of interfacial layers between naphthenic acid from oil and divalent cations from the aqueous phase. Also some studies on interfacial charging due to adsorption of ionic species have been reported.[18−20] However, how the insights obtained from studies with individual (cat/an)ions translate to the case of their mixtures remains to be seen. For example, ions of the same charge could compete with each other, perhaps following a Hofmeister series,[21] but alternatively they might also show synergistic effects.

To contribute to this underexplored field, we performed an experimental study aimed at the formation of solid interfacial layers, with particular focus on the role of the aqueous phase composition. The latter is varied extensively via the pH, the salt concentration, and the occurrence of mono- and divalent cations. Various combinations of cations are considered, from individual types like Na^+, Mg^{2+}, and Ca^{2+} to the complexity of artificial seawater.[22] To reduce the complexity of the overall system, the oil phase is represented by a model fluid of stearic acid ($CH_3(CH_2)_{16}COOH$) dissolved in *n*-decane ($CH_3(CH_2)_8CH_3$).

Fatty acid monolayers spread at the water/air (W/A) interface have been studied for many different aspects: the orientation and ordering of the molecules,[23,24] incorporation of metal ions in the film,[25−27] formation of super lattice structures,[28−30] viscoelastic properties,[31,32] phase transitions,[33−36] film stability,[37] Langmuir−Blodgett mono- and multilayer deposition,[24,38,39] and monolayer collapse.[40−44] The behavior of fatty acids at water/oil (W/O) interfaces has been investigated much less often, and studies have mainly been restricted to their absorption behavior.[1] Interestingly, the case of water in contact with oil presents additional degrees of freedom, like the solubility of surfactants and/or their precursors in bulk oil. This means that the formation of interfacial layers might also occur via different mechanisms.

We follow the interfacial behavior of the stearic acid molecules and their associated metal complexes by performing dynamic (i.e., time dependent) interfacial tension measurements using the pendant drop technique. Different stages of layer formation will be identified and discussed, based on the signature of the interfacial tension and its dependence on the compositions of the oil and the aqueous phase. The ultimately formed layers are mechanically characterized via the interfacial dilatational moduli, while the elemental composition and the presence of specific functional groups are accessed by X-ray photoelectron and infrared spectroscopy.

In particular, we will demonstrate that layer formation of metal stearates occurs through distinct stages. Deprotonation of the stearic acid is an enabling step for the whole sequence. For subphases containing both mono- and divalent cations, the formation is initiated by the monovalent ions, while in later stages the divalent ions become dominant. As a result, in the mixtures layers are formed through a kinetics that is different than that for the individual valencies, but always leading to thick solid layers in the end.

2. MATERIALS AND METHODS

Chemicals and Solutions. All chemicals are purchased from Sigma-Aldrich. Ultrapure water with a resistivity of 18.2 MΩ cm is obtained from a Millipore Synergy UV instrument. Artificial seawater[22] (see Table 1 for the composition) is prepared by mixing solutions of individual salts of ACS reagent grade. The pH of this solution varies between 7.5 and 8.0. Aqueous phase samples of the individual salts $CaCl_2$, $MgCl_2$, and NaCl are prepared at 1 M and diluted to the required concentrations, after which the pH is adjusted with KOH or HCl. To remove any undissolved impurities, all salt solutions are passed through a 1 μm filter. Anhydrous *n*-decane (purum grade, viscosity 0.9 mPa s) is cycled five times through a column with basic aluminum oxide (150 mesh) to remove surface active impurities that might originate from native residues or oxidation processes.[45] A 1 mM stearic acid (StA) stock solution in *n*-decane is prepared and diluted to the required concentrations.

Table 1. Composition of Artificial Seawater

type of cation	salt	concn in aqueous solution (mM)
monovalent	NaCl	426
	Na_2SO_4	29.4
	KCl	9.45
	$NaHCO_3$	2.43
	KBr	0.857
	H_3BO_3	0.438
	NaF	0.0744
divalent	$MgCl_2 \cdot 6H_2O$	55.5
	$CaCl_2 \cdot 2H_2O$	10.8
	$SrCl_2 \cdot 6H_2O$	0.0937

Dynamic Interfacial Tension Experiments. Pendant drop experiments are executed with an OCA 20L contact angle measuring and contour analysis system and analyzed with SCA 22 pendant drop software (both from DataPhysics). During and after injection of a drop of aqueous phase with a volume of 10−30 μL into a large amount of ambient oil phase, a movie is recorded at 50 frames/s. The time required to make a stable drop amounts to 1 s. The video recording allows to monitor the layer formation at the water/decane interface online from the moment it becomes visible and to obtain the evolution of the interfacial tension (IFT) offline. The latter is achieved by fitting the contour of the drop to the Young−Laplace equation combined with the hydrostatic pressure equation. Bond numbers (the ratio between buoyancy and interfacial tension forces) vary generally from 0.1 to 1, which enables this approach.[46] Since the drops have typical curvature radii in the millimeters range, the obtained IFTs generally compare well to those measured for truly planar interfaces.[47]

Interfacial Rheology Experiments. To investigate the onset and advancement of dilatational surface viscoelasticity, oscillating drop experiments are executed with the OCA 20L with an ODG 20 oscillating droplet generator extension and analyzed with SCA 26 oscillation/relaxation software (DataPhysics). A pendant drop of aqueous phase with a volume of 15−25 μL is formed in an ambient oil phase. A movie is recorded at 50 frames/s while the drop volume is oscillated sinusoidally at 1 Hz driven by a piezo element. The frequency of 1 Hz was chosen slightly higher than usual for this type of measurement[48] to obtain a better time resolution in measuring the transient phenomena in layer formation. Consequently, the measured interfacial moduli can become slightly overestimated.[49] In our case, a reference measurement on a bare water/decane interface (at 1 Hz) gave E' values ≪5 mN/m, which is indeed nonzero, but still much smaller than the values found for our solid interfacial layers.

The time-dependent drop area and interfacial tension (IFT) are extracted from the contour of the drop in individual movie frames. The relative interfacial area variation dA/A is kept below 0.05 to remain in the linear viscoelastic regime. From the mean values and amplitudes of the sinusoidal oscillations in drop area (A_0 and $\tilde{A}$) and interfacial tension (γ_0 and $\tilde{\gamma}$) and the phase shift (δ) between the two responses, the average IFT and the dilatational interfacial moduli are determined:[50,51]

$$E^* = E' + iE'' = \frac{\tilde{\gamma}}{\tilde{A}/A_0} e^{i\delta} \quad (1)$$

where E', the interfacial dilatational storage (elastic) modulus, measures the energy stored during a periodic deformation of the interface, and E'', the interfacial dilatational loss (viscous) modulus, accounts for energy

dx.doi.org/10.1021/la2010562 |*Langmuir* 2011, 27, 8738–8747

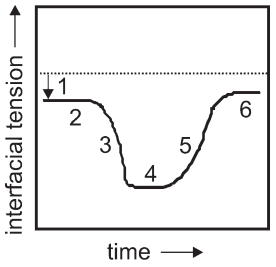

Figure 1. Typical evolution of the interfacial tension after an aqueous salt solution and a stearic acid solution in decane are brought into contact. The horizontal dashed line indicates the IFT of the pure water/decane interface.

dissipation due to relaxation processes. Measurements of E' and E'' are performed in 10 s intervals, using five oscillation cycles per measurement.

Multilayer Preparation. Layers are allowed to form for 2 h at a planar interface between an aqueous phase and a solution of stearic acid in decane. After transfer to a silicon wafer by dipping and retracting the latter, the sample is washed with ultrapure water to remove excess salt and subsequently air-dried before characterization. Because of the rapidly evolving, initially very thin and fragile layers at the liquid−liquid interface, we have only been able to transfer and analyze the layers in stage 6. These layers are characterized by scanning electron microscopy, X-ray photoelectron spectroscopy, and infrared spectroscopy.

Scanning Electron Microscopy. SEM micrographs are made in a JEOL 5610 field emission gun SEM, using an acceleration voltage of 0.55 kV and an inlens detector.

X-ray Photoelectron Spectroscopy (XPS). The XPS measurements, in which the elemental composition of the sample is measured from the kinetic energies of the electrons that escape upon X-ray irradiation, are performed using a Quantera SXM instrument (Physical Electronics).

Infrared (IR) Spectroscopy. IR absorption spectroscopy is performed on the layers transferred to a silicon wafer. Reference spectra for pure stearic acid and pure calcium stearate (CaSt) are obtained by grinding these compounds with KBr powder and pressing the mixture into a pellet. The IR measurements are performed using a Tensor FTIR spectrometer (Bruker). The presence of functional groups is identified by comparison of peaks with the reference samples and with literature data.

3. RESULTS

Distinct Stages in the Formation of Interfacial Layers. The behavior of the interfacial tension as a function of the time lapsed after the first contact between aqueous salt solution and stearic acid in decane turns out to be qualitatively similar in most cases. It comprises a number of steps, which are illustrated in Figure 1. After creating a fresh water/oil interface, one can observe an instantaneous IFT decrease (1) from the tension of pure water/decane to a plateau (2) with an IFT value that depends on the compositions of the fluids. The actual decline cannot be observed due to the finite formation time of the pendant drop. The existence of a plateau is suggestive of an adsorption equilibrium. At the end of the lag time, a sharp decrease in IFT (3) is observed, indicating a rapid and drastic change, which we interpret as a structural transition (see section 4). Then after a period with minor IFT changes (4), the IFT increases again (5). Sometimes this increase evolves to another plateau value (6). The characteristic times of the successive stages and the values of the IFT acquired depend on the compositions of the aqueous phase and the oil phase. The conditions also determine when the formation of an interfacial layer becomes visible to the naked eye. In experiments in which both [StA] and pH are high, layer formation is already observed in stage 3, while in experiments with low [StA], layer formation is only observed at the end of stage 5.

The decrease and subsequent increase of the IFT in stages 3−5 is often such a strong effect that it can be directly observed from the stretching and subsequent retraction of the drop (at constant volume) in the image-time series. This confirms that the formation of a visible surface layer initially does not interfere too much with the optical measurement of the drop contour (as needed to calculate the "IFT"). Dependent on the conditions, very thick solid layers can be observed at the end of stage 5. Under these conditions a reliable IFT cannot be obtained from the fitted drop contour. Apparent IFT data that are affected by this uncertainty are excluded from our analysis.

Effect of Stearic Acid Concentration and pH. The interfacial tension of the bare decane/water interface is close to 50 mN/m. When drops of demineralized water are formed in ambient decane with stearic acid concentrations ranging from 1 to 1000 μM, the IFT shows only a minor instantaneous effect. Subsequently, we find a weak decrease in interfacial tension with time, which depends weakly on the StA concentration in the oil phase (results not shown). On the basis of earlier observations with liquids that were used as received, we attribute this slowly decreasing IFTs to either remaining impurities in the system (in the aqueous phase or in the purified decane) or to very small amounts of adsorbed StA. In any case, it is clear that the stearic acid is barely interfacially active when dissolved in oil and brought into contact with demineralized water.

However, when artificial seawater is used to form the drops, the stearic acid dissolved in the decane does show interfacial activity, and the characteristic IFT response can be observed (Figure 2a). For [StA] $\leq$ 10 μM, the interfacial tension decreases only slightly with time. The amount of stearic acid might be too low to induce multilayer formation; however, one might also argue that the system is still in its lag time at the end of the experiment. However, for [StA] $\geq$ 30 μM the stages 1−5 can clearly be discerned (compare Figure 2a with Figure 1). For [StA] > 100 μM the formation of an interfacial layer even becomes visible to the naked eye within 1000 s (the typical duration of our experiments). Our observations clearly indicate that with increasing stearic acid concentration the IFT value at the plateau, the lag time, and the achieved minimum IFT all decrease, while the steepness of the IFT decrease and the extent of layer formation increase.

The difference in behavior for drops of demineralized water and ASW could be caused by differences in the ionic strength, the presence of specific ions, or the pH. While demineralized water has a pH of about 5.5 due to dissolution of carbon dioxide from the air, artificial seawater has a slightly elevated pH (~7.5−8) due to the presence of sodium bicarbonate. To investigate the effect of pH, drops of artificial seawater at various (adjusted) pH values are formed in ambient decane with 100 μM stearic acid (Figure 2b). The characteristic response is observed starting at a pH of 6. The effect of increasing the pH of ASW (Figure 2b) is remarkably similar to that of increasing [StA] at elevated pH (Figure 2a). From this observation we can conclude that the deprotonation of the stearic acid is a crucial step in interfacial layer formation.

Effect of Cation Valency and Salt Concentration. Since artificial seawater contains a variety of cations, each of which could in principle form a chemical complex with stearate anions, it is still not clear how the observed layers are formed. To examine the possibility that either mono- or divalent cations are

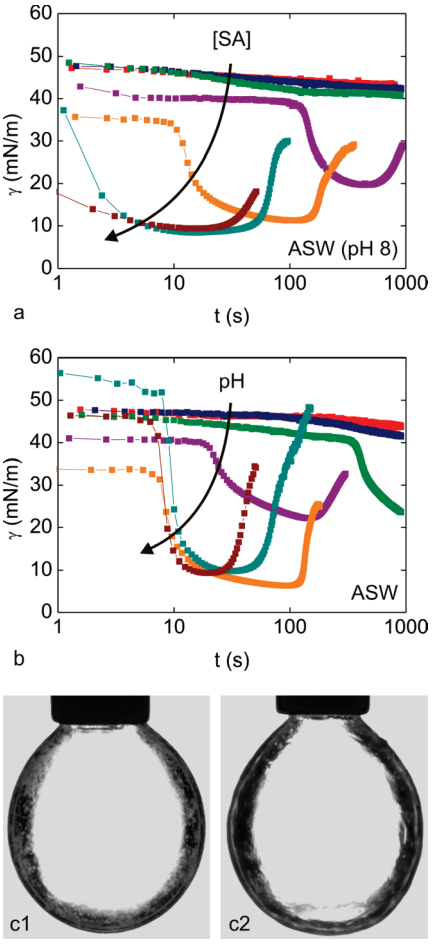

Figure 2. Interfacial tension versus time for (a) a drop of artificial seawater (pH 8) in ambient decane with various concentrations of stearic acid: 1 μM (red), 3 μM (blue), 10 μM (green), 30 μM (purple), 100 μM (orange), 300 μM (cyan), and 1000 μM (brown); and (b) a drop of artificial seawater in ambient decane with 100 μM stearic acid, at various pH values of the aqueous phase: pH 4 (red), pH 5 (blue), pH 6 (green), pH 7 (purple), pH 8 (orange), pH 9 (cyan), and pH 10 (brown). We remark that $Mg(OH)_2$ precipitation cannot be excluded at pH = 10. (c) Layer formation after creation of an interface between artificial seawater (pH 8) and decane with 1 mM stearic acid, (c1) after 15 min and (c2) after 40 min (note the somewhat crumpled structure of the drop surface).

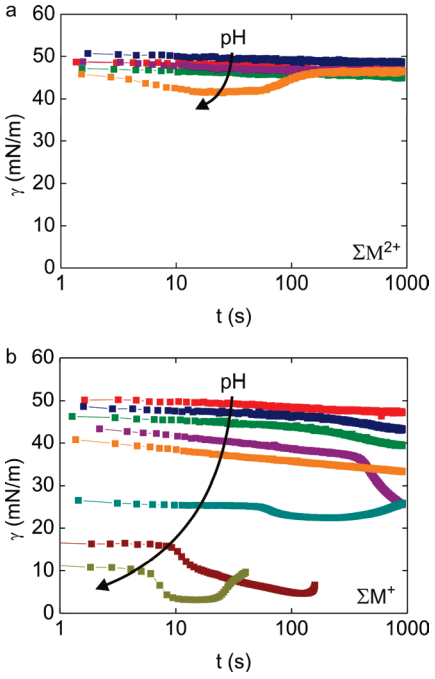

Figure 3. Interfacial tension versus time for aqueous drops in contact with a 100 μM stearic acid solution in decane. The aqueous phase consists of exclusively (a) the divalent cations and (b) the monovalent cations of ASW. In both graphs the pH of ASW is varied: pH 4 (red), pH 5 (blue), pH 6 (green), pH 7 (purple), pH 8 (orange), pH 9 (cyan), pH 10 (brown), and pH 11 (olive).

responsible, we prepare two solutions: one with all the monovalent cations of ASW and another with all the divalent ions. The concentrations of the individual cations are identical to those in Table 1. To explore also the pH dependence, relatively small amounts of KOH or HCl (<2% in total molarity) are added (as explained in section 2). After bringing these solutions into contact with an oil phase consisting of 100 μM stearic acid in decane, the time-dependent IFT is measured as before. The results are shown in Figure 3.

Remarkably, in case of the divalent cations (ΣM^{2+}, Figure 3a), the changes in IFT are only minor. The IFT shows only a small instantaneous decrease, which grows only slightly as the pH is increased from 4 to 9. For pH < 8, the IFT remains essentially constant. For pH = 8 and 9 the initial decrease is followed up by a small increase. For pH = 10 the typical IFT response with stages 1−5 is observed (result not shown), but for these conditions, the system is above the solubility limit of $Mg(OH)_2$.

For the monovalent cations (ΣM^{+}, Figure 3b), the IFT signature looks rather different. The instantaneous IFT decrease is again pH dependent, as for ΣM^{2+}, but the magnitude of the effect is much larger. For pH ≥ 7 the stages 1−3 of Figure 1 can be recognized. Apparently, the monovalent cations of ASW are needed to induce interfacial layer formation; changing the IFT in the typical way as sketched in Figure 1. However, the changes in IFT occurring in stage 3 are clearly less pronounced as those for ASW. This suggests that the thermodynamic driving force for further structural transitions (after the initial adsorption) is relatively small for the ΣM^{+} ions. Thus, in ASW the ΣM^{2+} ions are expected to be involved in the subsequent stages (see section 4).

Another noteworthy observation for the monovalent cations is that layer formation is visually observed (within the time span of the experiment) only at pH ≥ 10. Apparently, the kink in the IFT curve that marks the beginning of stage 3, is correlated to multilayer formation. This is not unexpected, since the transition from a 2D tot a 3D layer is generally a discontinuous one. What is however surprising, is that the bulk pH at which it happens is much higher than for ASW. This points at a synergistic effect of ΣM^{2+} and ΣM^{+} ions in ASW (see section 4).

In an attempt to further disentangle the cation contributions, additional experiments are conducted, now using aqueous subphases that contain (almost) exclusively Ca^{2+}, Mg^{2+}, or Na^{+} as the cation species. The concentration of their chloride salts was chosen to be 100 mM, to allow direct comparison between the three cations. Moreover, this concentration is also much larger than the $[K^{+}]$ (<1 mM) originating from the KOH that was used to adjust the pH, which was also varied.

The pendant drop results in Figures 4a,b show essentially a lack of IFT response for the subphases of both $CaCl_2$ or $MgCl_2$ up

dx.doi.org/10.1021/la2010562 |*Langmuir* 2011, 27, 8738–8747

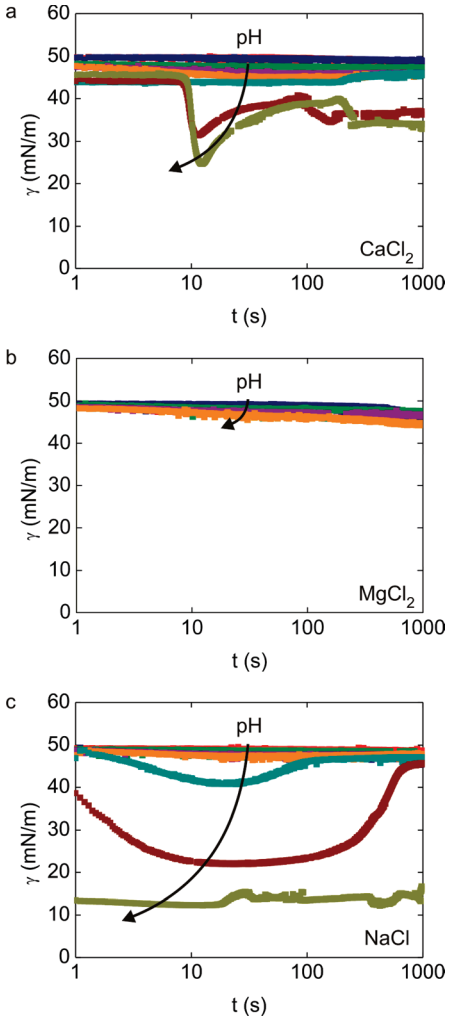

Figure 4. Interfacial tension versus time for aqueous drops with 100 mM (a) $CaCl_2$, (b) $MgCl_2$, and (c) NaCl, in ambient decane with 100 μM stearic acid, at various pH values of the aqueous phase: pH 4 (red), pH 5 (blue), pH 6 (green), pH 7 (purple), pH 8 (orange), pH 9 (cyan), pH 10 (brown), and pH 11 (olive).

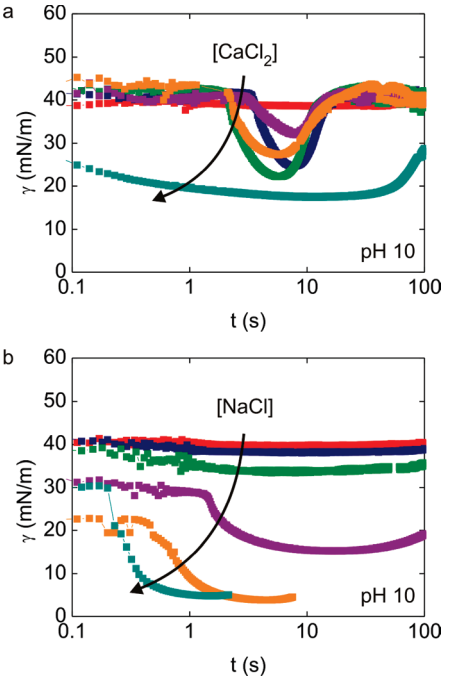

Figure 5. Interfacial tension versus time for aqueous drops at pH 10 in contact with ambient decane containing 1 mM stearic acid. The aqueous phase contains (a) $CaCl_2$ and (b) NaCl. Concentrations of these salts are 0.01 mM (red), 0.1 mM (blue), 1 mM (green), 10 mM (purple), 100 mM (orange), and 1000 mM (cyan). Note that the zero of the time axis is defined as the point where the drop just has been formed. The injection itself takes typically 1 s.

to pH = 8. This seems consistent with the findings in Figure 3a. For pH $\geq$ 9 we do not consider solutions at $[Mg^{2+}]$ = 0.1 M due to the possibility of $Mg(OH)_2$ precipitation at the O/W interface. For the Ca^{2+} solutions, the pH can be increased much further without this problem. For pH $\geq$ 10 the characteristic IFT response is observed for the Ca^{2+} ions (albeit stage 4 is missing). It clearly indicates that in absence of all the other (cat)ions of ASW the aqueous phase pH has to be much higher, in order to obtain interfacial layers. Again this points to a synergistic effect of the ΣM^{2+} and ΣM^{+} ions in ASW.

The response in case of a subphase of NaCl (Figure 4c) only weakly resembles the response for the fraction with monovalent cations (Figure 3b). Considering the strong dominance of Na^+ in the ΣM^+ mixture, one might expect much more similar behaviors in Figures 3b and 4c. However, this appears not to be the case. For the 0.1 M NaCl solution, the pH dependence of the IFT(time) function is weaker than for the ΣM^+ mixture at $\approx$0.5 M. Besides that, also the detailed shapes of the IFT-time graphs are different. This is in spite of the fact that the [StA] is the same, i.e. 100 μM. Comparing the IFT signatures for the subphase NaCl to those of $CaCl_2$ suggests that the mechanisms of initial layer formation are different for Na^+ or Ca^{2+} ions.

Finally, experiments are also performed for aqueous drops with various concentrations of $CaCl_2$ and NaCl at pH 10, in ambient decane with 1 mM stearic acid (Figure 5). At this high [StA], the duration of the IFT plateau (stage 2 in Figure 1) is reduced to O(1 s); this confirms that the accumulation of stearate species at the interface (as needed for the subsequent structural transition) proceeds more quickly for higher [StA] in the oil. For the subphases containing $CaCl_2$, two remarkable observations are made: both the immediate IFT decrease and the lag time remain more or less constant, as the Ca^{2+} concentration is varied from 0.1 to 100 mM. Apparently, the $[Ca^{2+}]$ does not play a key role in the kinetics of initial layer formation—at least not in this concentration range and pH. At the highest $[Ca^{2+}]$ of 1 M, the IFT signature has changed, suggesting a different mechanism of layer formation.

At all $[Ca^{2+}]$ > 10 μM, solid layer formation is visually observed: above 100 mM within 1000 s and longer for lower $[Ca^{2+}]$. This indicates that the growth rate of the layer does depend on $[Ca^{2+}]$ (in contrast to the formation rate of the initial layer). For the subphases of NaCl, the response is much more dependent on the salt concentration. At the highest $[Na^+]$ (>100 mM), the IFT even becomes so low that it passes the minimum value that is needed to counteract the gravity force on the drop (i.e., keep the drop attached).

Interfacial Dilatational Rheology. For a drop of artificial seawater dispersed in decane with a stearic acid concentration as high as 1 mM, the accumulation of material on the water/decane interface can be visually observed (as in Figure 2c) within several

dx.doi.org/10.1021/la2010562 |*Langmuir* 2011, 27, 8738–8747

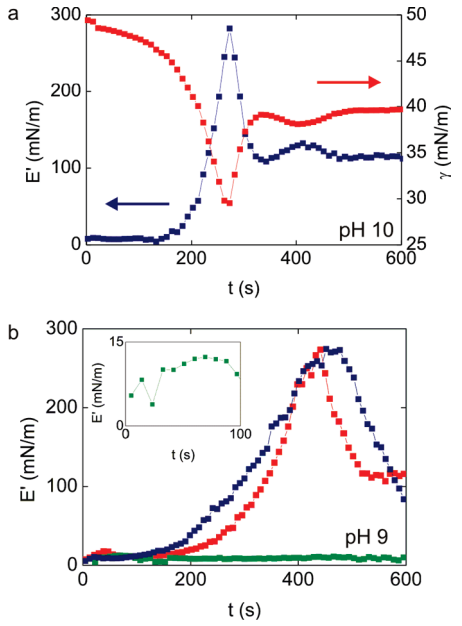

Figure 6. (a) Dilatational storage modulus E' (blue) and interfacial tension γ (red) versus time for an aqueous drop of 1 M $CaCl_2$ (pH 10) in ambient decane with 10 μM stearic acid. (b) E' versus time for aqueous drops (pH 9) of artificial seawater (red), 1 M $CaCl_2$ (blue), and 1 M NaCl (green) in ambient decane with 10 μM stearic acid. The inset shows the result for NaCl in close-up.

seconds after creation of the interface. Distinguishable individual patches nucleate and grow until the interface is fully covered. At longer time scales, the layer collapses and starts to buckle. Since the time scales of these processes are shorter than the 10 s time resolution of the oscillating drop technique, we adjust the concentration of stearic acid in decane to 10 μM. As aqueous phases we explore artificial seawater and 1 M aqueous solutions of $CaCl_2$ or NaCl at pH 9 or 10.

Figure 6a shows the IFT and the dilatational storage modulus E' versus time for an aqueous drop of 1 M $CaCl_2$ at pH 10 (in ambient decane with 10 μM StA). The onset of the viscoelastic behavior coincides with the sharp decrease in interfacial tension, and when the IFT is at its minimum, a maximum E' of about 300 mN/m is reached. Subsequently, the (apparent) interfacial tension increases again, while the elasticity decreases. E' continues to decrease over time, reaching a value of about 30 mN/m after 4 h (not shown). Visibility of the layer is reached only after several hours at this low [StA]. The maximum magnitude of E' (well above the IFT of bare water/decane) indicates that the dilatational elasticity has to originate (mainly) from the stretching of a (solid like) elastic surface layer.

We remark here that drops covered by such an elastic shell provide a case that is fundamentally different from that of classic adsorption layers and which gives rise to deviations from the Laplacian drop shape. For a modulus of 100 mN/m and IFT of 50 mN/m (roughly comparable to our case), these deviations have been predicted to be still small.[11,52] However, this also implies that very accurate shape measurements are needed for simultaneously extracting the values of γ and E' in this regime. Therefore, although the shape deviations are small in our measurements, the obtained values of γ and E' should no longer be taken as truly quantitative measures, in cases that solid layers are present.

An additional observation at pH of 10 is that the total harmonic distortion (the power of all higher harmonics divided by the power at the fundamental frequency) in the interfacial area oscillation occasionally shows a steep increase shortly after the start of the increase in E'. This loss of linearity in the mechanical response indicates that even for small imposed deformations ($dA/A < 0.05$), the surface layer cannot maintain its structural integrity, as a solid. Figure 6b shows the dilatational storage modulus for aqueous drops of artificial seawater and 1 M $CaCl_2$ and NaCl at pH 9 (in ambient decane with 10 μM stearic acid). The Ca^{2+} cations and ASW show similar results, while in case of NaCl only a slight increase in elasticity is observed. The maximum storage modulus of about 12 mN/m is reached quickly after the creation of the water/decane interface and remains fairly constant afterward. The loss modulus (not shown) shows considerable variation among experiments but is generally much smaller than the storage modulus, with a maximum value of about 50 mN/m for the divalent cations and about 10 mN/m for the monovalent cation. The layers formed at pH = 9 did not show the brittleness that is sometimes encountered at pH = 10.

SEM Imaging. In Figure 7, SEM pictures of the surfaces of layers made from subphases of ASW, 0.5 M $CaCl_2$ (pH 9), and 0.5 M $MgCl_2$ (pH 9) in contact with a 2 mM solution of StA in decane are shown. Large plateaus of several hundreds of nanometers in height can be seen on all surfaces. The morphology of the layers made using ASW is very different from the layers made using solutions of either $CaCl_2$ or $MgCl_2$. Besides that, it is noted that the plateaus formed in the presence of Mg^{2+} are higher than for Ca^{2+}.

XPS and IR Experiments. XPS spectra give information about the elemental composition of the interfacial layer formed after prolonged contact (i.e., in stage 6) between the aqueous and oil phases. The layers obtained from subphases containing either 0.5 M $CaCl_2$ or 0.5 M $MgCl_2$ (at pH 9) are used as references. The found elemental compositions (see Table 2) confirm the absence of other cations, while the levels of chloride indicate to which extent this anion could not be washed out (whereas metal stearates are not soluble, $CaCl_2$ is). Whereas for the sample from ASW the chloride content is insignificant, it is remarkably high for the subphase of $CaCl_2$. This is most likely due to precipitation of $CaCl_2$ during the drying step. Alternatively, also some CaCl-(St) complexes might be present.[53] In the sample from the $MgCl_2$ subphase, also some $Mg(OH)_2$ might be present.

Importantly, the layer formed from the subphase of artificial seawater (at pH 8) shows an elemental composition which is rather different from that of the aqueous subphase. Although magnesium is 5 times more abundant in artificial seawater than calcium, the amount of calcium that ends up in the interfacial layer exceeds the amount of magnesium by a factor of 20. Clearly, ultimately it is principally the calcium that is selectively incorporated.

Analysis of the same layers with IR spectroscopy serves to identify the chemical groups, in particular the ones involving the carboxyl unit. In the IR spectrum for pure stearic acid, the C═O stretching vibration of the carboxylic acid group is identified around 1710 cm^{-1} [54,55] (see also Figure 8a). This absorption peak is absent in all our layer samples (see Figure 8b), which clearly indicates that none of the layer samples contains significant amounts of (protonated) stearic acid. This result matches the expectation, since at the high pH where the layers are formed, nearly all acid groups should be ionized.

Ionized states of the carboxylate group can be identified from the C−O antisymmetric stretching vibration. For pure calcium stearate, the main peak is identified around 1580 cm^{-1}, while also

dx.doi.org/10.1021/la2010562 |*Langmuir* 2011, 27, 8738–8747

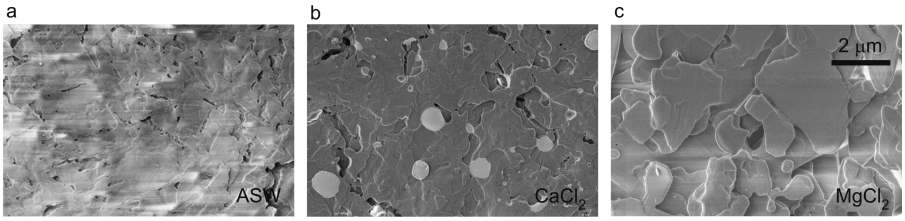

Figure 7. SEM images of the surface of layers grown at the interface between (a) ASW, or 0.5 M (b) $CaCl_2$ or (c) $MgCl_2$ solution (pH 9), and decane with 2 mM stearic acid.

Table 2. Relative Amounts of Different Elements Present in the Layers Grown at the Interface between an Aqueous Phase and Decane with 2 mM Stearic Acid As Determined by XPS[a]

element	ASW (pH 8)	0.5 M $CaCl_2$ (pH 9)	0.5 M $MgCl_2$ (pH 9)
C	48 ± 2	35 ± 3	46 ± 6
O	4.2 ± 0.2	3.2 ± 0.4	4.9 ± 0.7
Ca	1	1	
Mg	0.05 ± 0.07		1
Cl	0.02 ± 0.02	0.7 ± 0.2	0.16 ± 0.07

[a] Normalizations are made relative to the Ca for ASW and $CaCl_2$ and to Mg for $MgCl_2$. No sodium was detected.

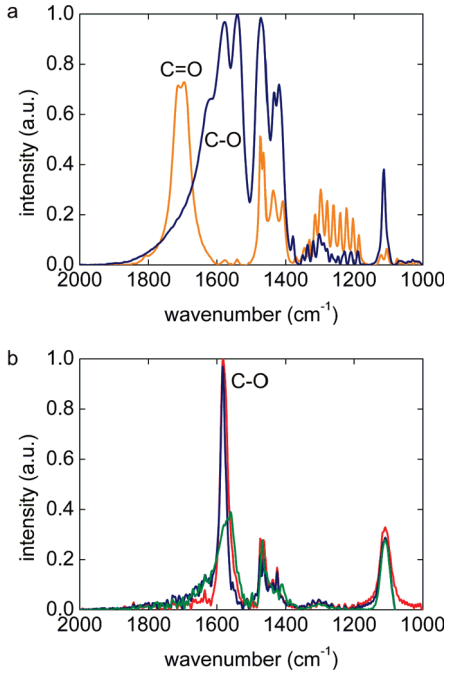

Figure 8. Part of the infrared spectra for (a) pure stearic acid (orange) and calcium stearate (blue), and (b) the layers grown at the interface between ASW (red), or 0.5 M $CaCl_2$ (blue) or $MgCl_2$ (green) solution (pH 9), and decane with 2 mM stearic acid.

a second peak is visible around 1540 cm^{-1}. This double peak has been assigned to a hydrated species and to the coexistence of carboxylate groups that interact with calcium ions in two different modes, namely unidentate (1580 cm^{-1}) and bidentate (1540 cm^{-1}).[54−56] In the spectrum of the layers prepared on a subphase of $CaCl_2$ or $MgCl_2$ (see Figure 8b) only the C−O antisymmetric stretching vibration around 1580 cm^{-1} is present. It turns out that the width of this peak depends on the metal ion that is associated with the carboxylate group: for layers created from the $MgCl_2$ subphase this peak is broadened (between 1560 and 1580 cm^{-1}) whereas with $CaCl_2$ it is not. Consequently, one can distinguish between calcium distearate and magnesium distearate. In the spectrum of the layer formed on a subphase of artificial seawater, the carboxylate peak is highly similar to the one present in the spectrum of the layer prepared on a subphase of $CaCl_2$. This corroborates our earlier XPS findings that the Ca^{2+} is selectively incorporated in the layer.

4. DISCUSSION AND INTERPRETATION

In our discussion of the formation of the interfacial layers of metal stearates, we refer to the first three stages that were distinguished in the typical response of the interfacial tension. Here we will focus on the most prominent trends in the data. We think that this is appropriate, considering the complexity of the layer formation in multicomponent mixtures, and the inherent limitations in insight that can be obtained, even from our combination of different techniques. On the basis of our observations (and literature) we speculate that the following general scenario could take place.

(i) Directly after the contact between the aqueous and oil phases, adsorption equilibria are set. The surface density of metal−stearate complexes is set by a dynamic exchange of cations and stearates between the interface and the bulk (aqueous respectively oil) phases. This is governed by equilibrium constants. In cases where multiple species can adsorb, the interfacial composition will be enriched by the species that have the strongest interfacial activity (i.e., thermodynamic driving force for adsorption). Stearate anions have a stronger interfacial activity than undissociated StA, and M^+ ions have a stronger interfacial activity than M^{2+} ions. The total surface density is low enough to allow new complexes to be formed at the interface.

These hypotheses are supported by the following observations. The IFT changes "instantaneously" (no transients could be observed) from the equilibrium value for bare water/decane to a lower value, after which it remains constant for some time. If diffusive transport of species from either side of the interface would be rate-limiting, then the IFT should show a steady decrease starting from about 50 mN/m. For the ASW subphase, the immediate decrease of the IFT grows with increasing [StA]. This adaptability of the IFT indicates that there is still room for more stearate species in the interfacial layer. The stronger IFT decrease for ΣM^+ as compared to ΣM^{2+} indicates that the former group creates species that are more interfacially active (in line with refs 1 and 17).

(ii) After the lag time plateau, nucleation and growth of a new phase occur. This is initiated at the interface, but the growth continues to take place in the third dimension (perpendicular to the interface). Here the subsequent layers will have an architecture that differs from the first

dx.doi.org/10.1021/la2010562 |*Langmuir* 2011, 27, 8738–8747

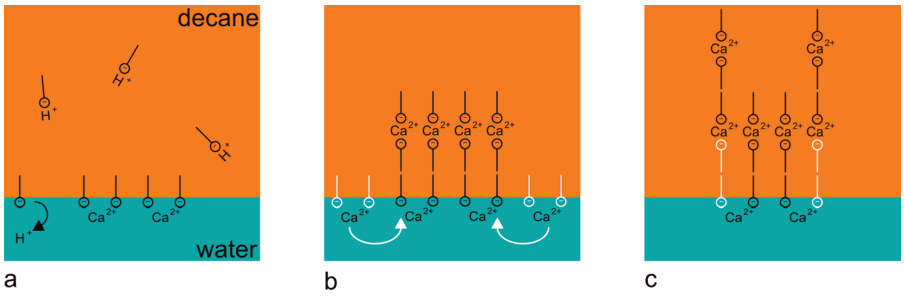

Figure 9. Proposed mechanism for multilayer formation. (a) Stearic acid molecules diffuse to the decane/water interface, deprotonate, and form metal−biacid complexes. (b) After nucleation of multilayer islands, new stearic acid molecules absorb onto the interface (c) and are subsequently incorporated in the interfacial layer. We note that this illustration is simplified. Chain orientations are taken equal in the first and subsequent layers, and the participation of monovalent ions in the initial stages is left out.

one and possibly also have a different chemical composition. Multilayers built up from divalent cations and stearate anions develop a high dilatational storage modulus because of a dense and ordered structure, which can store mechanical energy if deformed. Since this elastic behavior originates from short-ranged interactions, the layer behaves like a brittle solid shell. The subsequent decline of E' is due to the formation of cracks in the layer, which cannot heal anymore. These cracks also facilitate the further growth of the layer in the third dimension.

Nucleation and growth are suggested by the existence of a lag time, and the shorter duration hereof as the [StA] or the pH is increased. This behavior bears similarity to the precipitation of solids from bulk liquids. Here the new phase is more stable, but its formation involves an activation energy barrier, which gets lower as the monomer density ("supersaturation") increases. Differences in architecture between the first and subsequent layers are known to contribute[24,53] to the energy barrier. The formation of a solid phase of high chemical purity is suggested by our observations with XPS and IR. The solidlike behavior and brittleness are indicated by the large E' values and the low critical strain.

(iii) Growth of the layer continues as long as both cations and StA remain available in the bulk phases. New metal−stearates are then continually formed at the O/W interface. Formed calcium stearates reside in the oil phase in the form of stacked bilayers, with the aliphatic chains pointing outward in each bilayer.

This hypothesis is supported by the known tendency of calcium stearates to assume conformations in which the calcium ion is sandwiched between two stearates.[24] The main steps of the proposed mechanism of 3D layer formation and growth are illustrated in Figure 9.

Remarks on Artificial Seawater. While this proposed sequence of events could apply to several of the considered aqueous salt solutions (at sufficiently high pH) in contact with stearic acid solutions in decane, the observations with ASW as the aqueous subphase remain most intriguing. A remarkable synergy between the ΣM^+ and ΣM^{2+} ions appears to play a role. We speculate that in ASW the elemental composition of the interfacial layer changes in the course of time. The stronger interfacial activity of the stearates formed from monovalent cations, and especially the strong abundance of Na^+ in ASW, makes it likely that the initially adsorbed molecules are predominantly sodium stearates. Stearates of divalent cations are less interfacially active when occurring in the form of charged monostearate complexes. However, calcium distearates are thermodynamically more stable than any of the other stearates, at least as a bulk phase. The circumstance that as individually adsorbed species the sodium stearates are more stable, but as a collective bulk phase the calcium stearates are, implies that strong changes in cation composition must take place during the development of the layer. Different mechanisms would be possible, e.g., "heterogeneous nucleation" of $CaSt_2$ on top of a NaSt monolayer or replacement of Na by Ca in the first layer, followed by "homogeneous nucleation". In both scenario's, the synergy could have a strong effect on the kinetics of layer formation, as observed in the present study.

Remarks on the Influence of pH. One aspect that remains to be understood is why the bulk pH required to obtain solid layers in ASW is so much lower than the required bulk pH in solutions of individual salts. This observation should be seen in the light of possible differences between the pH in bulk aqueous phase and the pH at/near the interface. Such differences are known to occur if the interface is charged. In this case, electrostatic attraction and repulsion will modulate the local distributions of the ions in the solution, including the protons. The ionic strength of the subphase and specific ion effects influence the proton distribution and hence the local pH.[57−59] The sign and magnitude of the interfacial charge are set by the absorbed species, which can be negative (stearate anions), neutral (stearates of monovalent cations or distearates of divalent cations), or positive (monostearates of divalent cations). Knowledge of which of these species adsorb at which stage of the layer formation would be needed to further understand the dependence on subphase pH. This cannot be assessed with the methods we used and hence explanation of this issue has to fall beyond the scope of this paper.

5. CONCLUSIONS AND OUTLOOK

The formation of metal stearate layers at oil/water interfaces proceeds via distinct stages. Deprotonation of stearic acid is always required to initiate the multistep process. Immediate adsorption of surface active species is followed by molecular rearrangements that lead to the nucleation of a surface phase. Subsequently, layers are formed that continue to grow as multilayers inside the oil phase. The details of these scenarios are strongly dependent on the pH and cationic composition of the aqueous subphase. Stearates of monovalent cations appear to have stronger interfacial activity, but solid phases formed from them are thermodynamically less stable as compared to stearates of divalent cations, in particular Ca^{2+}. As a consequence,

dx.doi.org/10.1021/la2010562 |*Langmuir* 2011, 27, 8738–8747

although the stages leading to the final layers appear to be common, the underlying mechanisms are different for monovalent cations, divalent cations, and their mixtures. This is best illustrated in artificial seawater, in which layer formation is strongly facilitated by synergistic effects of the mono- and divalent cations.

We also like to mention some remaining and new questions. First, it remains to be fully understood why the required pH for the formation of thick layers is so much higher for either mono- or divalent cations, than for ASW. This is most probably related to differences in the accumulated charge density at the interface and to the ion distributions in the associated Stern and diffuse layers. Characterization with (e.g.) infrared reflection−adsorption spectroscopy could perhaps shed more light on this issue. Second, the details of the nucleation and growth of the layers remain obscure. Visualization by imaging ellipsometry at the oil/water interface might allow monitoring this process. And third, the response of the (developing) stearate layer to compositional changes in the fluids could be studied to gain more insight into the formation and mechanical properties of the layers. For this, microfluidics could be used.

■ ASSOCIATED CONTENT

Supporting Information. Full infrared spectra. This material is available free of charge via the Internet at http://pubs.acs.org.

■ AUTHOR INFORMATION

Corresponding Author
*E-mail: r.deruiter-1@tnw.utwente.nl.

■ ACKNOWLEDGMENT

We thank BP for financial support. Barbara Mojet (Catalytic Processes and Materials, University of Twente) is kindly acknowledged for IR spectroscopy and Arun Banpurkar for layer preparations. We also thank Agata Brzozowska and Daniel Ebeling for discussions.

■ REFERENCES

(1) Brandal, O.; Sjoblom, J.; Oye, G. Interfacial behavior of naphthenic acids and multivalent cations in systems with oil and water. I. A pendant drop study of interactions between n-dodecyl benzoic acid and divalent cations. *J. Dispersion Sci. Technol.* **2004**, *25* (3), 367–374.

(2) Havre, T. E.; Ese, M. H.; Sjoblom, J.; Blokhus, A. M. Langmuir films of naphthenic acids at different pH and electrolyte concentrations. *Colloid Polym. Sci.* **2002**, *280* (7), 647–652.

(3) Binks, B. P.; Kellay, H.; Meunier, J. Bending elastic-modulus of monolayers at oil-water interfaces. *Thin Solid Films* **1992**, *210* (1−2), 118–120.

(4) Bonfillon, A.; Langevin, D. Viscoelasticity of monolayers at oil-water interfaces. *Langmuir* **1993**, *9* (8), 2172–2177.

(5) Dickinson, E. Adsorbed protein layers at fluid interfaces: interactions, structure and surface rheology. *Colloids Surf., B* **1999**, *15* (2), 161–176.

(6) Aske, N.; Orr, R.; Sjoblom, J. Dilatational elasticity moduli of water-crude oil interfaces using the oscillating pendant drop. *J. Dispersion Sci. Technol.* **2002**, *23* (6), 809–825.

(7) Jeribi, M.; Almir-Assad, B.; Langevin, D.; Henaut, I.; Argillier, J. F. Adsorption kinetics of asphaltenes at liquid interfaces. *J. Colloid Interface Sci.* **2002**, *256* (2), 268–272.

(8) Ferri, J. K.; Kotsmar, C.; Miller, R. From surfactant adsorption kinetics to asymmetric nanomembrane mechanics: Pendant drop experiments with subphase exchange. *Adv. Colloid Interface Sci.* **2010**, *161* (1−2), 29–47.

(9) Li, J. B.; Zhang, Y.; Yan, L. L. Multilayer formation on a curved drop surface. *Angew. Chem., Int. Ed.* **2001**, *40* (5), 891–894.

(10) Lu, G.; Chen, H.; Li, J. B. Forming process of folded drop surface covered by human serum albumin, beta-lactoglobulin and beta-casein, respectively, at the chloroform/water interface. *Colloids Surf., A* **2003**, *215* (1−3), 25–32.

(11) Ferri, J. K.; Dong, W. F.; Miller, R.; Mohwald, H. Elastic moduli of asymmetric ultrathin free-standing polyelectrolyte nanocomposites. *Macromolecules* **2006**, *39* (4), 1532–1537.

(12) Martin, R. L.; Winters, J. C. Composition of crude oil through seven carbons as determined by gas chromoatogrpahy. *Anal. Chem.* **1959**, *31* (12), 1954–1960.

(13) Westlake, D. W.; Jobson, A.; Phillipp., R.; Cook, F. D. Biodegradability and crude-oil composition. *Can. J. Microbiol.* **1974**, *20* (7), 915–928.

(14) Meredith, W.; Kelland, S. J.; Jones, D. M. Influence of biodegradation on crude oil acidity and carboxylic acid composition. *Org. Geochem.* **2000**, *31* (11), 1059–1073.

(15) Lager, A.; Webb, K. J.; Collins, I. R. In *LoSal Enhanced Oil Recovery: Evidence of Enhanced Oil Recovery at the Reservoir Scale*; SPE/DOE Symposium on Improved Oil Recovery, Tulsa, OK, 2008.

(16) Seccombe, J.; Lager, A.; Jerauld, G.; Jhaveri, B.; Buikema, T.; Bassler, S.; Denis, J.; Webb, K. J.; Cockin, A.; Fueg, E. In *Demonstration of Low-Salinity EOR at Interwell Scale, Endicott Field, Alaska*; SPE Improved Oil Recovery Symposium, Tulsa, OK, 2010.

(17) Brandal, O.; Sjoblom, J. Interfacial behavior of naphthenic acids and multivalent cations in systems with oil and water. II: Formation and stability of metal naphthenate films at oil-water interfaces. *J. Dispersion Sci. Technol.* **2005**, *26* (1), 53–58.

(18) Bonfillon, A.; Sicoli, F.; Langevin, D. Dynamic surface-tension of ionic surfactant solutions. *J. Colloid Interface Sci.* **1994**, *168* (2), 497–504.

(19) Danov, K. D.; Vlahovska, P. M.; Kralchevsky, P. A.; Broze, G.; Mehreteab, A. Adsorption kinetics of ionic surfactants with detailed account for the electrostatic interactions: effect of the added electrolyte. *Colloids Surf., A* **1999**, *156* (1−3), 389–411.

(20) Ivanov, I. B.; Marinova, K. G.; Danov, K. D.; Dirnitrova, D.; Ananthapadmanabhan, K. P.; Lips, A. Role of the counterions on the adsorption of ionic surfactants. *Adv. Colloid Interface Sci.* **2007**, *134−35*, 105–124.

(21) Zhang, Y. J.; Cremer, P. S. Interactions between macromolecules and ions: the Hofmeister series. *Curr. Opin. Chem. Biol.* **2006**, *10* (6), 658–663.

(22) Kester, D. R.; Duedall, I. W.; Connors, D. N. Pytkowic.Rm, Preparation of artificial seawater. *Limnol. Oceanogr.* **1967**, *12* (1), 176–179.

(23) Gericke, A.; Huhnerfuss, H. The effect of cations on the order of saturated fatty-acid monolayers at the air-water-interface as determined by infrared reflection-absorption spectrometry. *Thin Solid Films* **1994**, *245* (1−2), 74–82.

(24) Peng, J. B.; Barnes, G. T.; Gentle, I. R. The structures of Langmuir-Blodgett films of fatty acids and their salts. *Adv. Colloid Interface Sci.* **2001**, *91* (2), 163–219.

(25) Langmuir, I. S.; V., J. Composition of Fatty Acid Films on water Containing Calcium or Barium Salts. *J. Am. Chem. Soc.* **1936**, *58* (2), 284–287.

(26) Bloch, J. M.; Yun, W. B.; Yang, X.; Ramanathan, M.; Montano, P. A.; Capasso, C. Adsorption of counterions to a stearate monolayer spread at the water-air interface - a synchrotron x-ray study. *Phys. Rev. Lett.* **1988**, *61* (26), 2941–2944.

(27) Yazdanian, M.; Yu, H.; Zografi, G. Ionic interactions of fatty-acid monolayers at the air-water-interface. *Langmuir* **1990**, *6* (6), 1093–1098.

(28) Kmetko, J.; Datta, A.; Evmenenko, G.; Dutta, P. The effects of divalent ions on Langmuir monolayer and subphase structure: A grazing-incidence diffraction and Bragg rod study. *J. Phys. Chem. B* **2001**, *105* (44), 10818–10825.

(29) Dupres, V.; Cantin, S.; Benhabib, F.; Perrot, F.; Fontaine, P.; Goldmann, M.; Daillant, J.; Konovalov, O. Superlattice formation in fatty

acid monolayers on a divalent ion subphase: Role of chain length, temperature, and subphase concentration. *Langmuir* **2003**, *19* (26), 10808–10815.

(30) Pignat, J.; Cantin, S.; Liu, R. C. W.; Goldmann, M.; Fontaine, P.; Daillant, J.; Perrot, F. pH-dependent kinetics of MgCl2 adsorption under a fatty-acid Langmuir film. *Eur. Phys. J. E* **2006**, *20* (4), 387–394.

(31) Yazdanian, M.; Yu, H.; Zografi, G.; Kim, M. W. Divalent-cation stearic acid monolayer interactions at the air-water interface. *Langmuir* **1992**, *8* (2), 630–636.

(32) Ghaskadvi, R. S.; Carr, S.; Dennin, M. Effect of subphase Ca++ ions on the viscoelastic properties of Langmuir monolayers. *J. Chem. Phys.* **1999**, *111* (8), 3675–3678.

(33) Shih, M. C.; Bohanon, T. M.; Mikrut, J. M. Pressure and pH-dependence of the structure of a fatty-acid monolayer with calcium-ions in the subphase. *J. Chem. Phys.* **1992**, *96* (2), 1556–1559.

(34) Kaganer, V. M.; Mohwald, H.; Dutta, P. Structure and phase transitions in Langmuir monolayers. *Rev. Mod. Phys.* **1999**, *71* (3), 779–819.

(35) Cantin, S.; Péralta, S.; Fontaine, P.; Goldmann, M.; Perrot, F. Evolution toward the X Phase of Fatty Acid Langmuir Monolayers on a Divalent Cation Solution. *Langmuir* **2010**, *26* (2), 830–837.

(36) Johann, R.; Vollhardt, D.; Mohwald, H. Shifting of fatty acid monolayer phases due to ionization of the headgroups. *Langmuir* **2001**, *17* (15), 4569–4580.

(37) Aveyard, R.; Binks, B. P.; Carr, N.; Cross, A. W. Stability of insoluble monolayers and ionization of Langmuir-Blodgett multilayers of octadecanoic acid. *Thin Solid Films* **1990**, *188* (2), 361–373.

(38) Neuman, R. D.; Swanson, J. W. Multilayer deposition of stearic acid-calcium stearate mono-molecular films. *J. Colloid Interface Sci.* **1980**, *74* (1), 244–259.

(39) Gönen, M.; Öztürk, S.; Balköse, D.; Okur, S.; Ülkü, S. Preparation and Characterization of Calcium Stearate Powders and Films Prepared by Precipitation and Langmuir-Blodgett Techniques. *Ind. Eng. Chem. Res.* **2010**, *49* (4), 1732–1736.

(40) Neuman, R. D. Stearic acid and calcium stearate monolayer collapse. *J. Colloid Interface Sci.* **1976**, *56* (3), 505–510.

(41) Angelova, A.; Vollhardt, D.; Ionov, R. 2D-3D transformations of amphiphilic monolayers influenced by intermolecular interactions: A Brewster angle microscopy study. *J. Phys. Chem.* **1996**, *100* (25), 10710–10720.

(42) Kundu, S.; Datta, S.; Hazra, S. Effect of metal ions on monolayer collapses. *Langmuir* **2005**, *21* (13), 5894–5900.

(43) Kundu, S.; Langevin, D. Fatty acid monolayer dissociation and collapse: Effect of pH and cations. *Colloids Surf., A* **2008**, *325* (1−2), 81–85.

(44) Seok, S.; Kim, T. J.; Hwang, S. Y.; Kim, Y. D.; Vaknin, D.; Kim, D. Imaging of Collapsed Fatty Acid Films at Air-Water Interfaces. *Langmuir* **2009**, *25* (16), 9262–9269.

(45) Goebel, A.; Lunkenheimer, K. Interfacial tension of the water/n-alkane interface. *Langmuir* **1997**, *13* (2), 369–372.

(46) Alvarez, N. J.; Walker, L. M.; Anna, S. L. A non-gradient based algorithm for the determination of surface tension from a pendant drop: Application to low Bond number drop shapes. *J. Colloid Interface Sci.* **2009**, *333* (2), 557–562.

(47) Banpurkar, A. G.; Nichols, K. P.; Mugele, F. Electrowetting-based microdrop tensiometer. *Langmuir* **2008**, *24* (19), 10549–10551.

(48) Miller, R.; Ferri, J. K.; Javadi, A.; Kragel, J.; Mucic, N.; Wustneck, R. Rheology of interfacial layers. *Colloid Polym. Sci.* **2010**, *288* (9), 937–950.

(49) Leser, M. E.; Acquistapace, S.; Cagna, A.; Makievski, A. V.; Miller, R. Limits of oscillation frequencies in drop and bubble shape tensiometry. *Colloids Surf., A* **2005**, *261* (1−3), 25–28.

(50) Myrvold, R.; Hansen, F. K. Surface elasticity and viscosity from oscillating bubbles measured by automatic axisymmetric drop shape analysis. *J. Colloid Interface Sci.* **1998**, *207* (1), 97–105.

(51) Ravera, F.; Loglio, G.; Kovalchuk, V. I. Interfacial dilational rheology by oscillating bubble/drop methods. *Curr. Opin. Colloid Interface Sci.* **2010**, *15* (4), 217–228.

(52) Ferri, J. K. F. P. A. L. Axisymmetric Drop Shape Analysis with Anisotropic Interfacial Stresses: Deviations from the Young-Laplace Equation. In *Bubble and Drop Interfaces*; Miller, R., Liggieri, L., Eds.; Brill: Leiden, 2011; Vol. 2, pp 61−74.

(53) Garoff, S.; Deckman, H. W.; Dunsmuir, J. H.; Alvarez, M. S.; Bloch, J. M. Bond-orientational order in Langmuir-Blodgett surfactant monolayers. *J. Phys.* **1986**, *47* (4), 701–709.

(54) Bagg, J.; Haber, M. D.; Gregor, H. P.; Abramson, M. B.; Fichman, M. Composition of stearic acid monolayers from calcium-containing substrates. *J. Am. Chem. Soc.* **1964**, *86* (14), 2759.

(55) Deamer, D. W.; Meek, D. W.; Cornwell, D. G. Properties composition and structure of stearic acid-stearate monolayers on alkaline earth solutions. *J. Lipid Res.* **1967**, *8* (3), 255.

(56) Lu, Y. Q.; Miller, J. D. Carboxyl stretching vibrations of spontaneously adsorbed and LB-transferred calcium carboxylates as determined by FTIR internal reflection spectroscopy. *J. Colloid Interface Sci.* **2002**, *256* (1), 41–52.

(57) Le Calvez, E.; Blaudez, D.; Buffeteau, T.; Desbat, B. Effect of cations on the dissociation of arachidic acid monolayers on water studied by polarization-modulated infrared reflection-absorption spectroscopy. *Langmuir* **2001**, *17* (3), 670–674.

(58) Miranda, P. B.; Du, Q.; Shen, Y. R. Interaction of water with a fatty acid Langmuir film. *Chem. Phys. Lett.* **1998**, *286* (1−2), 1–8.

(59) Eijkel, J. C. T.; van den Berg, A. Nanofluidics and the chemical potential applied to solvent and solute transport. *Chem. Soc. Rev.* **2010**, *39* (3), 957–973.